Earth, Moon, and Planets (2022) 126: 5
https://doi.org/10.1007/s11038-022-09547-5

Statistical Thermodynamics of Surface-Bounded Exospheres

Norbert Schörghofer[1,2]

Received: 21 November 2021 / Accepted: 20 April 2022 / Published online: 12 May 2022

Abstract
Neutral exospheres of large airless bodies consist of atoms or molecules on ballistic trajectories. An import example is the lunar water exosphere, thought to transport water to cold traps. In anticipation of future observational measurements, the theory of thermalized surface-bounded gravitationally-bound exospheres is further developed. The vertical density profile is calculated using thermodynamic averages of an ensemble of ballistic trajectories. When the launch velocities follow the Maxwell–Boltzmann Flux distribution, the classical density profile results. For many other probability distributions, including thermal desorption from a vertical wall, the density diverges logarithmically near the surface. Hence, an exosphere resulting from thermal desorption from a rough surface includes a ground-hugging population that appears to be colder than the surface. Another insight derived from the thermodynamic perspective is that cold traps can be interpreted in terms of the frost-point of the water exosphere, if the long-term average of the pressure of the exosphere is considered. Ice in lunar caves is long-lasting only if the cave interior is below the cold trap temperature threshold.

Keywords Exosphere · The Moon · Cold traps · water

1 Introduction

The Moon, Mercury, and other large airless bodies have rarefied atmospheres, which are collisionless exospheres (e.g., H_2, He, Ar, and H_2O) where neutral atoms and molecules follow ballistic trajectories (Killen and Ip 1999; Stern 1999). One particularly important example is the putative water exosphere of the Moon, because it can potentially transport water from any location on the surface to the cold traps (Watson et al. 1961a, b; Arnold 1979; Schorghofer et al. 2021). A water group exosphere (H_2O or OH) has been detected on the Moon by Benna et al. (2019), but many of its properties remain unknown.

Atoms and molecules can initially be ejected by thermal or non-thermal process. They then either escape to space or fall back onto the surface. The vibrational frequency of the bond with the substrate surface is typically 10^{13} Hz (De Jong and Niemantsverdriet 1990),

✉ Norbert Schörghofer
norbert@psi.edu

[1] Planetary Science Institute, Tucson, AZ, USA

[2] Planetary Science Institute, Honolulu, HI, USA

so a particle should quickly thermalize, take on the temperature of the surface, leave with a thermal velocity distribution, and undergo a sequence of ballistic hops (Watson et al. 1961b; Hurley et al. 2016). Some, usually minor, fraction bounces elastically instead (Haynes et al. 1992). The vertical density profile can be calculated from the distribution of launch velocities.

Numerous Monte-Carlo simulations have been carried out for the water exospheres of Mercury and the Moon (e.g., Butler 1997; Crider and Vondrak 2002; Schorghofer 2014; Prem et al. 2018; Kloos et al. 2019; Feoktistova et al. 2021). The goal here is to develop the continuum theory with a solid surface boundary condition. Exospheres above a dense atmosphere, such as on Earth and the Sun, have long been investigated theoretically (e.g., Öpik and Singer 1959; Johnson and Fish 1960; Aamodt and Case 1962; Chamberlain 1963; Shen 1963). With a solid surface as lower boundary condition, the velocity distribution may be different and the number of particles is fixed or limited rather than supplied from a reservoir (i.e., a closed rather than an open thermodynamic system). Here, a first-principle approach is used for gravitationally-bound exospheres with thermal launch velocities that is ideally suited for the surface-bounded case and fully analytically tractable.

2 Thermodynamics of Ballistic Trajectories

2.1 Temperature of an Exosphere

To the extent molecules thermalize with the surface, the temperature of the exosphere is *exactly* the same as the temperature of the surface. This follows from the very concept of temperature (the zeroth law of thermodynamics). An ensemble of ballistic trajectories in thermal equilibrium with the surface has by definition the same temperature as the reservoir it is in equilibrium with.

The literature on exobase-bounded exospheres includes discussions on how the velocity distribution changes with height above the surface and how a (local) temperature should be defined in this collisionless environment. For surface-bounded exospheres, the answer is simple and straightforward, although the temperature is assigned to the whole ensemble rather than at each height.

If the surface has multiple temperatures, as it practically always has, the temperature of the exosphere is a linear superposition of these individual temperatures, averaged over a footprint the size of the hop distance. Strong lateral temperature heterogeneity is caused by shadows, but on most of the dayside, shadows cover only a minor portion of the surface (Hayne et al. 2021).

2.2 Single Ballistic Hop

Let v_z denote the *initial* vertical velocity component. It follows from elementary mechanics that for constant g the duration of ballistic flight is

$$t_D = \frac{2v_z}{g} \tag{1}$$

and the maximum height of a ballistic trajectory is

$$z_{\max} = \frac{v_z^2}{2g} \tag{2}$$

The vertical velocity as a function of time and height, respectively, is

$$\frac{dz}{dt} = v_z - gt = \sqrt{v_z^2 - 2gz} \tag{3}$$

The time the particle spends at a particular height z is proportional to $1/\mid dz/dt \mid$. Therefore, the density profile for a single ballistic hop is

$$\rho(z) = \frac{g}{v_z} \frac{1}{\sqrt{v_z^2 - 2gz}} \tag{4}$$

where the prefactor was determined from normalization:

$$\int_0^{z_{\max}} \rho(z)\, dz = 1 \tag{5}$$

To obtain a mass density, ρ has to be multiplied with the column-integrated mass.

2.3 Ensemble Averages

Although an exosphere is collisionless, the trajectories still represent a thermodynamic ensemble (i.e., a statistical ensemble in equilibrium) as the particles thermalize with the surface. Given a probability distribution of initial velocities $P(v_z)$, the ensemble average of a quantity X per hop is

$$\langle X \rangle = \int XP(v_z)\, dv_z \tag{6}$$

The time average for a stationary exosphere, $\langle\langle . \rangle\rangle$, has to be weighted by the flight duration and is

$$\langle\langle X \rangle\rangle = \int XP(v_z) \frac{t_D}{\langle t_D \rangle}\, dv_z = \int XP(v_z) \frac{v_z}{\langle v_z \rangle}\, dv_z \tag{7}$$

Both types of averages are properly normalized: $\langle 1 \rangle = 1$ and $\langle\langle 1 \rangle\rangle = 1$. Note that the factor $v_z / \langle v_z \rangle$ represents a cosine-dependence, and

$$\langle\langle X \rangle\rangle = \frac{\langle v_z X \rangle}{\langle v_z \rangle} \tag{8}$$

For the density on the surface ($z = 0$), Eqs. (4) and (7) imply

$$\langle\langle \rho(0) \rangle\rangle = \frac{g}{\langle v_z \rangle} \int_0^\infty \frac{1}{v_z} P(v_z)\, dv_z \tag{9}$$

When the probability distribution is expanded as $P(v_z) = P(0) + P'(0)v_z + ...$, then $\langle\langle \rho(0) \rangle\rangle < \infty$ requires $P(0) = 0$. If $P(0) > 0$ (and P is analytic), the surface density diverges.

To form the average of the vertical density profile, the integration is over all initial velocities that are sufficiently high to reach a given height, i.e., $v_z > \sqrt{2gz}$. The time-averaged profile $\langle\langle \rho \rangle\rangle$ is

$$\langle\langle \rho \rangle\rangle = \int \rho(z;v_z) P(v_z) \frac{v_z}{\langle v_z \rangle} \, dv_z = \frac{g}{\langle v_z \rangle} \int_{\sqrt{2gz}}^{\infty} \frac{1}{\sqrt{v_z^2 - 2gz}} P(v_z) \, dv_z \tag{10}$$

where (4) was used. The same result is obtained if one considers that the time spent in a height interval is proportional to the inverse of the instantaneous velocity $1/\mid dz/dt \mid$. Hence,

$$\langle\langle \rho \rangle\rangle = \frac{g}{\langle v_z \rangle} \int_{\sqrt{2gz}}^{\infty} \frac{1}{\mid dz/dt \mid} P(v_z) \, dv_z = \frac{g}{\langle v_z \rangle} \left\langle \frac{1}{dz/dt} \right\rangle \tag{11}$$

With (3) this also results in (10). The density profile is an ensemble average over the inverse of the vertical component of the launch velocity.

2.4 Velocity Distribution for Thermal Desorption

The "Knudsen cosine law" applies to the velocity distribution of a rarefied gas near a wall (Knudsen 1909; Comsa 1968) and states that the probability of an angle of emergence varies as the cosine of the angle with the surface normal. This experimentally determined fact can be explained theoretically, if the direction in which a molecule rebounds from a solid wall is independent of the direction it approaches the wall (Knudsen 1909). This is the opposite of the velocity correlation expected for specular reflection on a smooth surface. The decorrelation can be understood in terms of the dispersing microgeometry of the wall (Feres and Yablonsky 2004) or from thermalization during contact.

The probability distribution derived by Armand (1977) is based on the oscillations of atoms in the crystal:

$$P_3 \, d^3v = \frac{2\beta^2}{\pi} v_z e^{-\beta(v_x^2+v_y^2+v_z^2)} \, dv_x dv_y dv_z \tag{12}$$

with

$$\beta = \frac{m}{2kT} \tag{13}$$

where k is the Boltzmann constant, T the temperature associated with the initial velocities, and m the mass of the atom or molecule. The Armand distribution obeys the Knudsen cosine law, because of the prefactor v_z.

Based on numerical simulations, Smith et al. (1978) and Hodges (1980) realized that launch velocities with a Maxwell–Boltzmann distribution do not result in the expected density profile and proposed that the launch velocities for an exobase correspond to a "Maxwell–Boltzmann flux" (MBF) distribution, which places an extra factor of the vertical velocity component, v_z, in front of the Maxwell–Boltzmann distribution. A wall bordering a gas with Maxwell–Boltzmann velocity distribution experiences a MBF velocity distribution. The MBF distribution is identical to the Armand distribution (12).

Deviations from the cosine law have been measured (Comsa 1968). The detailed velocity distribution depends on the properties of the surface and the type of adsorption, but

the Armand/MBF distribution is the leading order description for thermal desorption from a surface (see also Hodges and Mahaffy 2016). Microrelief and diffusion can modify the effective residence times and angular distribution of launch velocities (Sarantos and Tsavachidis 2020, 2021). These phenomena are not considered in this work, although they might be important.

3 Exact Solutions for Vertical Density Profile

3.1 The Classical Density Profile

Separated in x, y, and z-components the Armand distribution (12) is

$$P_3 = \underbrace{\left(\sqrt{\frac{\beta}{\pi}}e^{-\beta v_x^2}\right)}_{P_B(v_x)}\underbrace{\left(\sqrt{\frac{\beta}{\pi}}e^{-\beta v_y^2}\right)}_{P_B(v_y)}\underbrace{\left(2\beta v_z e^{-\beta v_z^2}\right)}_{P_A(v_z)} \tag{14}$$

It is identical to the "Maxwell–Boltzmann flux" (MBF) distribution. The lateral velocity components follow Boltzmann distributions, P_B. The distribution of the vertical component ($v_z \geq 0$) is given by

$$P_A(v_z) = 2\beta v_z e^{-\beta v_z^2} \tag{15}$$

This functional form is also known as Rayleigh distribution, and compared to a Boltzmann distribution, $P_A = 2\sqrt{\pi\beta}v_z P_B$. Using Eqs. (6, 7, 15), averages for the Armand distribution are

$$\langle v_z \rangle_A = \frac{1}{2}\sqrt{\frac{\pi}{\beta}}, \quad \langle v_z^2 \rangle_A = \frac{1}{\beta} = \frac{2kT}{m}, \quad \langle\langle v_z \rangle\rangle_A = \frac{2}{\sqrt{\pi\beta}}, \quad \langle\langle v_z^2 \rangle\rangle_A = \frac{3}{2\pi\beta} \tag{16}$$

This velocity distribution allocates kT for the vertical translational mode (16), instead of $kT/2$.

It is useful to introduce the scale height

$$H = \frac{kT}{mg} = \frac{1}{2g\beta} \tag{17}$$

The averages of $z_{\max}$ (2) are

$$\langle z_{\max} \rangle_A = \frac{\langle v_z^2 \rangle_A}{2g} = H \qquad \text{and} \qquad \langle\langle z_{\max} \rangle\rangle_A = \frac{\langle\langle v_z^2 \rangle\rangle_A}{2g} = \frac{3}{2}H \tag{18}$$

The average maximum height per hop is H, whereas the maximum height reached by the particles in flight at any given time is $(3/2)H$. The average duration of a ballistic hop, using Eqs. (1), (6), and (15), is

$$\langle t_D \rangle_A = \frac{1}{g}\sqrt{\frac{\pi}{\beta}} = \sqrt{\frac{2\pi H}{g}} \tag{19}$$

The time-averaged density profile becomes

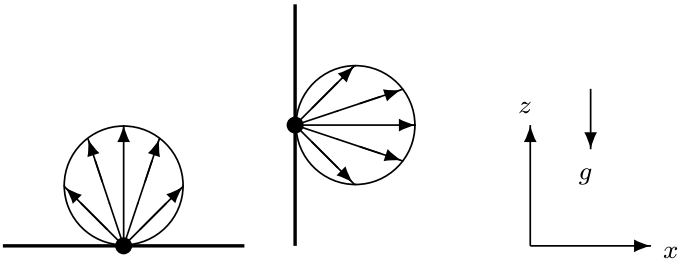

Fig. 1 Schematic illustration of the distribution of launch velocities from a horizontal and a vertical surface. Both use the same coordinate system, with z opposite the direction of gravity

$$\langle\langle \rho \rangle\rangle_A = \frac{1}{H} e^{-z/H} \tag{20}$$

This reproduces the barometric formula, even with the same scale height H as an isothermal hydrostatic atmosphere.

The classical particle-based (Öpik and Singer 1959; Shen 1963) and Liouville theorem based (Aamodt and Case 1962) derivations lead to the same density profile. To demonstrate this, one of their derivations is reproduced here for the simple case of constant gravitational acceleration. Shen (1963) writes the density profile as

$$\rho = 4\pi \left(\frac{\beta}{\pi}\right)^{3/2} \iint \frac{v_t v_z}{\sqrt{v_z^2 - 2gz}} e^{-\beta(v_z^2+v_t^2)} dv_t dv_z \tag{21}$$

Once the integral over the tangential velocity v_t from 0 to ∞ is carried out, this further integrates to

$$\rho = 2\left(\frac{\beta}{\pi}\right)^{1/2} \int_{\sqrt{2gz}}^{\infty} \frac{e^{-\beta v_z^2}}{\sqrt{v_z^2 - 2gz}} v_z dv_z = e^{-2\beta g z} = e^{-z/H} \tag{22}$$

This reproduces the barometric Equation (20), with a different normalization.

3.2 Divergent Density Profile

When desorption from a vertical wall is considered, the x and z velocity components in (14) are swapped (Fig. 1):

$$P_{3\perp} = \underbrace{\left(2\beta v_x e^{-\beta v_x^2}\right)}_{P_A(v_x)} \underbrace{\left(\sqrt{\frac{\beta}{\pi}} e^{-\beta v_y^2}\right)}_{P_B(v_y)} \underbrace{\left(2\sqrt{\frac{\beta}{\pi}} e^{-\beta v_z^2}\right)}_{P_\perp(v_z)} \tag{23}$$

The probability distribution of the vertical component of the initial velocity v_z is

$$P_\perp(v_z) = 2\sqrt{\frac{\beta}{\pi}}e^{-\beta v_z^2} \tag{24}$$

where a factor of 2 has been added, which ignores the downward moving molecules ($v_z \geq 0$), otherwise it is the same as P_B. Averages with respect to $P_\perp(v_z)$ are

$$\langle v_z \rangle_\perp = \frac{1}{\sqrt{\pi\beta}}, \quad \langle v_z^2 \rangle_\perp = \frac{1}{2\beta} = \frac{kT}{m} \tag{25}$$

The time-averaged density profile is

$$\langle\langle \rho \rangle\rangle_\perp = \int_{\sqrt{2gz}}^{\infty} \rho(z;v_z) P_\perp(v_z) \frac{v_z}{\langle v_z \rangle} dv_z = \frac{1}{2H} e^{-z/2H} K_0\left(\frac{z}{2H}\right) \tag{26}$$

where K_0 is the modified Bessel function of the second kind. For $z \ll H$, $K_0(z/2) = -\ln(z/4) - \gamma$, where γ is the Euler constant, and in this limit

$$\langle\langle \rho \rangle\rangle_\perp = -\frac{1}{2H}\left(\ln\left(\frac{z}{4H}\right) + \gamma\right) \quad \text{for} \quad z \ll H \tag{27}$$

which implies that the density near the surface goes to infinity at a logarithmic rate. This divergence was already anticipated by Eq. (9).

In the opposite limit of large height, $z \gg H$, $K_0(z/2) = \sqrt{\pi/z}\, e^{-z/2}$, and therefore

$$\langle\langle \rho \rangle\rangle_\perp = \frac{1}{2}\sqrt{\frac{\pi}{z}}\, e^{-z/H} \quad \text{for} \quad z \gg H \tag{28}$$

At large heights, the density falls off faster than an exponential.

In an exosphere, the mean free path is much larger than the scale height, so having a local density higher than the saturation vapor density is not unphysical. Figure 2 compares $\langle\langle \rho \rangle\rangle_A$ and $\langle\langle \rho \rangle\rangle_\perp$. What appears to be a "ground-hugging" population is actually part of a population described by a single temperature. Figure 3 illustrates the launch velocity distributions and the resulting density profiles.

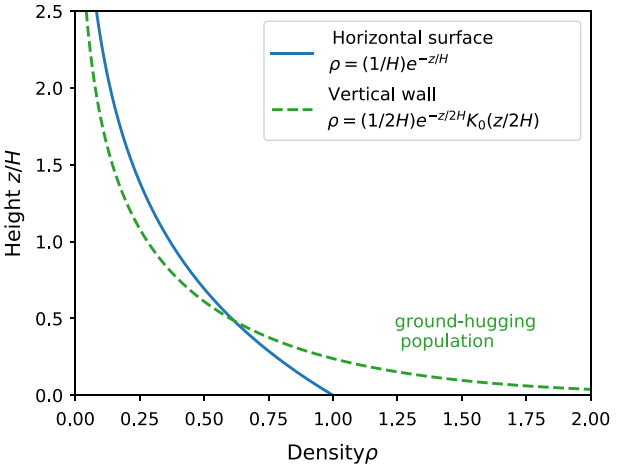

Fig. 2 Theoretical density profiles of exospheres according to Eqs. (20) and (26)

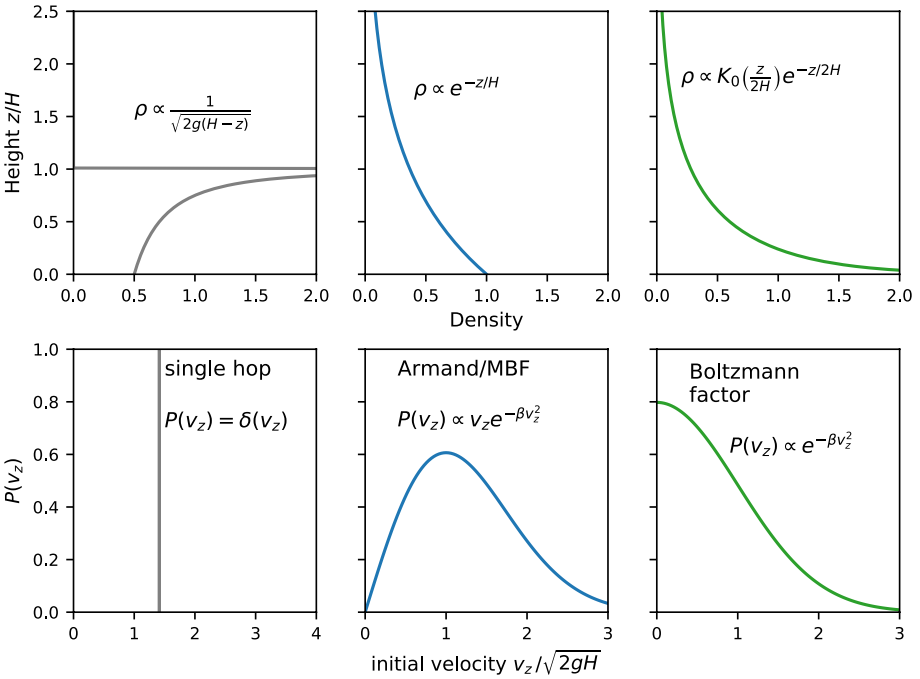

Fig. 3 Vertical velocity distributions and the resulting density profiles. Left row: With constant launch velocity (or a single launch), the time a molecule spends at each height increases with height (4), and most time is spent where it reverses direction. Middle row: An exponential density profile (20) results from an Armand/MBF distribution of initial velocities (15). Right row: If the vertical component of the launch velocity follows a Boltzmann distribution (24), the density profile diverges logarithmically near the surface (26), resulting in a "ground-hugging" population

As apparent from Eq. (9), the near-surface divergence arises from particles with small vertical launch velocities. Typically these will have small launch angles. On a rough surface, launches at small angles are blocked more often than launches at steep angles, which eliminates the divergence, but with a different height scale, and blocking does not erase the ground-hugging population.

The number of molecules delivered to a small vertical surface element by ballistic trajectories is expected to be about the same as for a horizontal surface. Hence, the slope dependence of the mass flux will approximately reflect that of the velocity probability distribution.

3.3 Rough Surfaces and Two-Component Exospheres

A planetary surface is rough on small scales, so the local surface normal rarely points along the direction of gravity. Roughness makes the launch velocities more isotropic. The density profile can be calculated in closed form for emission from vertical (Sect. 3.1) and horizontal (Sect. 3.2) surfaces. For a general slope angle, there does not appear to be a closed-form solution. For a rough surface, that contains both horizontal and vertical elements, the combined solution will have an exponential behavior for high altitudes and a faster-than-exponential (a ground-hugging) behavior near the surface. In this sense, the

exosphere can be thought of as consisting of two components: One that consists predominantly of fast particles ejected upwards from horizontal surfaces, and one that consists predominately of slowly ascending particles ejected from steep surfaces. However, they both have the same temperature and they are end-members of the same population rather than two distinct populations. In conclusion, particles launched from a rough surface according to the Armand/MBF distribution are expected to follow the classical density profile at high altitudes, but to have a more ground-hugging behavior at low altitudes.

The temperature of an exosphere is often inferred by fitting the density profile to an exponential, or to a more general solution that takes radial variations in g into account. In this case, the exospheric profile would be misinterpreted as consisting of a hot and a cold population (a two component exosphere), and the ground-hugging population would be assigned a temperature lower than the surface temperature. The transition between the two density profiles can be placed at $\langle\langle \rho(z) \rangle\rangle_A = \langle\langle \rho(z) \rangle\rangle_\perp$, which occurs at $z/H \approx 0.486$ (Fig. 2). Below this height, the combined density profile is dominated by the logarithmic divergence.

4 Relations Between Cold Traps, a Variable Exosphere, and Spelean Ice

Here the relation of an exosphere to its condensed phase is considered. The concepts are independent of the results for the vertical density profile in the previous section.

4.1 The Hertz-Knudsen-Langmuir Equation

The Hertz-Knudsen equation provides the sublimation loss of ice into vacuum (Persad and Ward 2016), and was already given in Langmuir (1913):

$$S = \frac{p_s}{\sqrt{2\pi kTm}} \tag{29}$$

where p_s is the saturation (equilibrium) vapor pressure. It is derived in the following way. Consider vapor and ice in equilibrium with each other. At the saturation vapor pressure, the flux from the vapor to the solid surface equals the flux in the opposite direction. In the absence of a collisional gas, the flux from the ice surface is still the same. The sublimation rate is therefore the same as the flux of an ideal gas with a Maxwell–Boltzmann velocity distribution toward a solid wall. The flux toward the surface is $n\bar{v}_z$, where n is the volumetric number density and the average is over the half of the molecules that move toward the solid surface, and n is the number density. For the Maxwell–Boltzmann distribution

$$\bar{v}_z = \frac{1}{2\sqrt{\pi\beta}} = \sqrt{\frac{kT}{2\pi m}} \tag{30}$$

Combined with the ideal gas law, $p_s = nkT$, this leads to Eq. (29).

Thermal desorption is expected to have the same distribution of launch velocities as sublimation from ice (Sect. 2.4), and hence the Hertz-Knudsen equation can be extended to a situation where p_s is not the equilibrium pressure over ice, but the equilibrium pressure over adsorbed H_2O.

4.2 The Vertical Flux

For a water exosphere above an ice-covered surface, the flux on the surface is the sublimation rate of ice into vacuum. In the stationary case, the net flux is zero, as an equal number of particles move up and down. The uni-directional flux on the surface is given by $F = (1/2)\rho v_z$. The ensemble-averaged flux is

$$\langle\langle F\rangle\rangle(z=0) = \frac{1}{2}\langle\langle \rho v_z\rangle\rangle = \langle\langle \frac{g}{2v_z}\rangle\rangle = \frac{g}{2\left\langle v_z\right\rangle} \tag{31}$$

For the Armand distribution

$$\langle\langle F\rangle\rangle_A(z=0) = \frac{mg}{\sqrt{2\pi mkT}} \tag{32}$$

This flux has units of inverse time and needs to be multiplied with the column abundance σ to get the column-integrated number of molecules.

For a gravitationally-bound water exosphere above an ice-covered surface $S = \sigma\langle\langle F\rangle\rangle$. Using (29) and (32), this leads to a simple relation for the column-integrated mass of the water exosphere of an ice-covered body:

$$m\sigma = \frac{p_s}{g} \tag{33}$$

which says that the weight of the exosphere equals the pressure at its base, although, in the absence of collisions above the surface, there are no force chains. The balance is physically reasonable, because, on average, the momentum of molecules impinging on the surface equals the momentum at which they are thermally desorbed. As mentioned above, this relation can be generalized from an ice surface to a surface with adsorbed H_2O, using the appropriate equilibrium pressure p_s.

4.3 Exospheres and Cold Traps

Exospheres can be related thermodynamically to the cold traps that they feed. Cold traps on airless bodies are areas where the sublimation loss into vacuum is negligible and water ice could therefore accumulate in them. More precisely, cold traps are areas where the sublimation loss is less than the amount delivered to the cold traps. The flux from an exosphere into the cold traps is related to the pressure of the exosphere, and therefore the pressure of the exosphere is related to the sublimation pressure of ice in a cold trap, as long as long-term averages are considered.

The Hertz-Knudsen Equation (29) makes clear that the sublimation rate into vacuum, S, depends on the saturation vapor pressure p_s. Both, S and p_s, are strictly monotonic functions of T. Figure 4 shows the phase diagram of H_2O with vacuum sublimation rates among the annotations, which illustrates the association of the cold trap temperature threshold with sublimation pressures.

The flux of vapor into the cold traps S_{exo}, averaged over a long time, exceeds S, and should be calculated based on the temperature surrounding the cold traps from where molecules launch into the cold traps. This flux varies greatly over time, but in the long

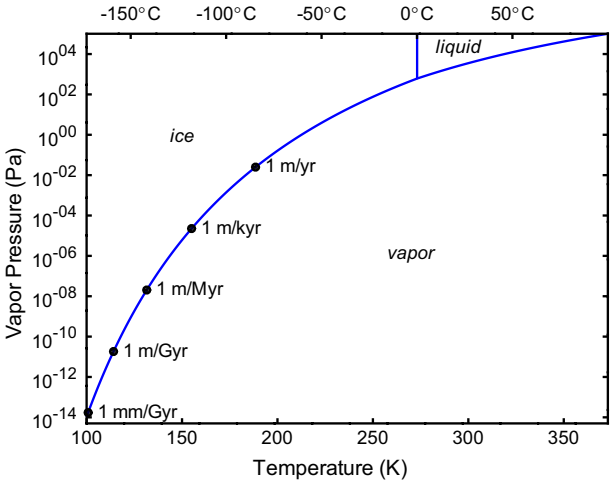

Fig. 4 Phase diagram of H_2O. Sublimation rates into vacuum are annotated along the vapor-solid line

term it is larger than the more steady sublimation loss from the cold traps. At the cold trap threshold temperature

$$S(T_{\text{thres}}) = \frac{1}{P}\int_0^P S_{\text{exo}}\, dt \tag{34}$$

where P is a long time period, perhaps as much as Gyrs. Using the Hertz-Knudsen relation,

$$\frac{p_s(T_{\text{thres}})}{\sqrt{T_{\text{thres}}}} = \frac{1}{P}\int_0^P \frac{p_{\text{exo}}}{\sqrt{T_{\text{sur}}}}\, dt \tag{35}$$

where T_{sur} is the (daytime) temperature of the surrounding area. Given that the saturation pressure varies exponentially with temperature (Fig. 4), the time variability of the denominator is reasonably neglected,

$$p_s(T_{\text{thres}}) \approx \sqrt{\frac{T_{\text{thres}}}{T_{\text{sur}}}}\frac{1}{P}\int_0^P p_{\text{exo}}\, dt \tag{36}$$

Therefore p_s at the cold trap threshold is slightly lower than but similar to the long-term average of the exospheric pressure. This leads to an insightful interpretation: The cold trap margins are close to the frost point of the water exosphere, as long as the long-term average is considered. The vertical axis in Fig. 4 can almost be interpreted as the long-term average of the exospheric pressure.

As a specific example, at 110 K the saturation pressure of crystalline ice (Murphy and Koop 2005) is about 3×10^{-12} Pa and the sublimation rate is 144 kg m^{-2} Gyr^{-1} or 0.15 m/Gyr. At 115 K these numbers are 3×10^{-11} Pa and 1.6 m/Gyr. Taking the latter temperature, the column abundance above the cold traps should be no more than 6×10^{14} molecules/m^2 according to Eq. (33). This is an upper limit, because only the margins of the cold traps will be at this temperature and the ice is often not even exposed on the surface. The actual number could well be several orders of magnitude lower. The exosphere quickly

spreads and this pressure should be present even at the equator. The spatial variations in pressure and column abundance over the dayside should be within a factor of only a few (Schorghofer 2015).

4.4 Geographic Limits to the Occurrence of Lunar Ice Caves

Caves can act as (subsurface) cold traps. A cave is traditionally defined as a cavity that is longer than the height and width of its entrance. Hence, water molecules typically have to hop multiple times to reach the end of a cave. Temperatures in the cave interior are shielded from peak surface temperatures and likely vary little over a lunation. Several cave entrance candidates have been identified on the Moon (e.g.,Haruyama et al. 2009; Robinson et al. 2012). Lunar caves that contain ice would be an exciting prospect. Mean surface temperatures on the Moon are below freezing globally (Williams et al. 2017), and subfreezing temperatures hence prevail at shallow depths.

In the long term, spelean ice is lost to space by sublimation. The mean free path is on the order of the cave diameter, so a cave does not provide much of a diffusion barrier that could delay this loss. (And if it did provide much of a diffusion barrier this would slow migration not only out of the cave but also into the cave.) However, if the temperature of the cave interior is below the cold trap temperature ($\lesssim 120$ K), it received more water molecules from the outside than it has lost. (As discussed above, the cold trap threshold approximately corresponds to the long-term average of the supply rate.) Hence, lunar spelean ice is likely limited to cave interiors colder than about 120 K, which restricts their potential occurrence to the polar regions, but includes regions far outside of cold traps. Cavities are expected even in the polar regions (e.g., Kring et al. 2021; Lee 2022). Topography induces major temperature variations, so areas colder than the threshold for mean temperature are not described by a single latitude threshold but made up of many disjoint regions.

5 Conclusions

Observations have not yet established to what extent surface-bounded exospheres of H_2O are in thermal equilibrium with the surface, but basics of the theory are worked out here. Thermalized surface-bounded exospheres are described by the temperature of the surface they are in contact with.

The vertical density profile of a stationary surface-bounded exosphere in a uniform gravity field can be calculated from the distribution of launch velocities, Eq. (10). For an Armand (Maxwell–Boltzmann-Flux) distribution, the density profile follows an exponential. From a vertical wall with the same launch velocities, the density approaches infinity near the surface at a logarithmic rate, Eq. (26). More generally, if $P(v_z)$ is the probability distribution of the vertical component of launch velocities (and the function is analytic), then $P(0) > 0$ implies the surface density diverges. These exact solutions suggest that thermal desorption from a rough surface will appear to result in two-component exospheres, although they are described by a single temperature.

Since the influx of molecules into cold traps is related to the pressure of a (water) exosphere, the cold trap temperature threshold can be interpreted as the frost point of the exosphere, as long as the long-term average of the exospheric pressure is considered, Eq. (36). Along the same line of argument, lunar ice caves will lose water if the cave interior is

above the cold trap temperature of about 120 K, which places geographic limits on the occurrence of spelean ice on the Moon.

Data Availability Statement No datasets were generated or analyzed during the current study.

Declarations

Conflict of Interest: The author declares no conflict of interest relevant to this study.

References

R.E. Aamodt, K.M. Case, Density in a simple model of the exosphere. Phys. Fluid **5**(9), 1019–1021 (1962)

G. Armand, Classical theory of desorption rate velocity distribution of desorbed atoms; possibility of a compensation effect. Surf. Sci. **66**(1), 321–345 (1977). https://doi.org/10.1016/0039-6028(77)90414-9

J.R. Arnold, Ice in the lunar polar regions. J. Geophys. Res. **84**(B10), 5659 (1979). https://doi.org/10.1029/JB084iB10p05659

M. Benna, D.M. Hurley, T.J. Stubbs, P.R. Mahaffy, R.C. Elphic, Lunar soil hydration constrained by exospheric water liberated by meteoroid impacts. Nat. Geosci. **12**(5), 333–338 (2019). https://doi.org/10.1038/s41561-019-0345-3

B.J. Butler, The migration of volatiles on the surfaces of mercury and the Moon. J. Geophys. Res. **102**(E8), 19283–19291 (1997)

J.W. Chamberlain, Planetary coronae and atmospheric evaporation. Planet. Space Sci. **11**(8), 901–960 (1963)

G. Comsa, Angular distribution of scattered and desorbed atoms from specular surfaces. J. Chem. Phys. **48**(7), 3235–3240 (1968)

D.H. Crider, R.R. Vondrak, Hydrogen migration to the lunar poles by solar wind bombardment of the Moon. Adv. Space Res. **30**, 1869–1874 (2002). https://doi.org/10.1016/S0273-1177(02)00493-3

A.M. De Jong, J.W. Niemantsverdriet, Thermal desorption analysis: Comparative test of ten commonly applied procedures. Surf. Sci. **233**(3), 355–365 (1990)

E.A. Feoktistova, A.Y. Zharkova, A.A. Kokhanov, Zh.F. Rodionova, Migration of water molecules in the permanently shaded areas of polar areas of Mercury. Earth, Moon, and Planets **125**, 5 (2021). https://doi.org/10.1007/s11038-021-09542-2

R. Feres, G. Yablonsky, Knudsen's cosine law and random billiards. Chem. Eng. Sci. **59**(7), 1541–1556 (2004). https://doi.org/10.1016/j.ces.2004.01.016

J. Haruyama, K. Hioki, M. Shirao, T. Morota, H. Hiesinger, et al. Possible lunar lava tube skylight observed by SELENE cameras. *Geophys Res Lett* 36(21): 2009. https://doi.org/10.1029/2009GL040635.

P.O. Hayne, O. Aharonson, N. Schörghofer, Micro cold traps on the Moon. Nat. Astr. **5**, 169–175 (2021). https://doi.org/10.1038/s41550-020-1198-9

D.R. Haynes, N.J. Tro, S.M. George, Condensation and evaporation of H2O on ice surfaces. J. Phys. Chem. **96**, 8502–8509 (1992)

R.R. Hodges, Methods for Monte Carlo simulation of the exospheres of the Moon and Mercury. J. Geophys. Res. **85**(A1), 164–170 (1980)

R.R. Hodges, P.R. Mahaffy, Synodic and semiannual oscillations of argon-40 in the lunar exosphere. Geophys. Res. Lett. **43**(1), 22–27 (2016). https://doi.org/10.1002/2015GL067293

D.M. Hurley, J.C. Cook, M. Benna, J.S. Halekas, P.D. Feldman et al., Understanding temporal and spatial variability of the lunar helium atmosphere using simultaneous observations from LRO, LADEE, and ARTEMIS. Icarus **273**, 45–52 (2016). https://doi.org/10.1016/j.icarus.2015.09.011

F.S. Johnson, R.A. Fish, The telluric hydrogen corona. Astrophys. J. **131**, 502–509 (1960)

R.M. Killen, W.-H. Ip, The surface-bounded atmospheres of Mercury and the Moon. Rev. Geophys. **37**(3), 361 (1999)

J.L. Kloos, J.E. Moores, J. Sangha, T.G. Nguyen, N. Schorghofer, The temporal and geographic extent of seasonal cold trapping on the Moon. J. Geophys. Res. Planets **124**(7), 1935–1944 (2019). https://doi.org/10.1029/2019JE006003

M. Knudsen, Die gesetze der molekularströmung und der inneren reibungsströmung der gase durch röhren. Ann. Phys. **333**(1), 75–130 (1909)

D.A. Kring, G.Y. Kramer, D.B.J. Bussey, D.M. Hurley, A.M. Stickle, C.H. van der Bogert, Prominent volcanic source of volatiles in the south polar region of the Moon. Adv. Space Res. **68**, 4691–4701 (2021). https://doi.org/10.1016/j.asr.2021.09.008

I. Langmuir, The vapor pressure of metallic tungston. Phys. Rev. **2**(5), 329–342 (1913)

P. Lee. Impact melt lava inflation fractures in Schomberger-A Crater, Moon: New permanently shadowed regions and possible caves near the lunar south pole. *Proc. Lunar Planet. Sci. Conf.*, 53: abstract #2685, 2022

D.M. Murphy, T. Koop, Review of the vapour pressures of ice and supercooled water for atmospheric applications. Q. J. Royal Meteorol. Soc. **131**(608), 1539–1565 (2005). https://doi.org/10.1256/qj.04.94

E.J. Öpik, S.F. Singer, Distribution of density in a planetary exosphere. Phys. Fluid. **2**, 653–655 (1959)

A.H. Persad, C.A. Ward, Expressions for the evaporation and condensation coefficients in the Hertz-Knudsen relation. Chem. Rev. **116**(14), 7727–7767 (2016). https://doi.org/10.1021/acs.chemrev.5b00511

P. Prem, D.B. Goldstein, P.L. Varghese, L.M. Trafton, The influence of surface roughness on volatile transport on the Moon. Icarus **299**, 31–45 (2018). https://doi.org/10.1016/j.icarus.2017.07.010

M.S. Robinson, J.W. Ashley, A.K. Boyd, R.V. Wagner, E.J. Speyerer, B.R. Hawke, H. Hiesinger, C.H. Van Der Bogert, Confirmation of sublunarean voids and thin layering in mare deposits. Planet. Space Sci. **69**(1), 18–27 (2012). https://doi.org/10.1016/j.pss.2012.05.008

M. Sarantos and S. Tsavachidis. The boundary of alkali surface boundary exospheres of Mercury and the Moon. *Geophys. Res. Lett.*, 47(16): 2020GL088930, 2020. https://doi.org/10.1029/2020GL088930.

M. Sarantos, S. Tsavachidis, Lags in desorption of lunar volatiles. Astrophys. J. Lett. **919**(2), L14 (2021). https://doi.org/10.3847/2041-8213/ac205b

N. Schorghofer, Migration calculations for water in the exosphere of the Moon: Dusk-dawn asymmetry, heterogeneous trapping, and D/H fractionation. Geophys. Res. Lett. **41**, 4888–4893 (2014). https://doi.org/10.1002/2014GL060820

N. Schorghofer, Two-dimensional description of surface-bounded exospheres with application to the migration of water molecules on the Moon. Phys. Rev. E (2015). https://doi.org/10.1103/PhysRevE.91.052154

N. Schorghofer, M. Benna, A.A. Berezhnoy, B. Greenhagen, B.M. Jones, S. Li, T.M. Orlando, P. Prem, O.J. Tucker, C. Wöhler, Water group exospheres and surface interactions on the Moon, Mercury, and Ceres. Space Sci. Rev. **217**, 74 (2021). https://doi.org/10.1007/s11214-021-00846-3

C.S. Shen, An analytic solution for density distribution in a planetary exosphere. J. Atmos. Sci. **20**(2), 69–72 (1963)

G.R. Smith, D.E. Shemansky, A.L. Broadfoot, L. Wallace, Monte Carlo modeling of exospheric bodies: Mercury. J. Geophys. Res. **83**(A8), 3783–3790 (1978)

S.A. Stern, The lunar atmosphere: history, status, current problems, and context. Rev. Geophys. **37**, 453–491 (1999)

K. Watson, B.C. Murray, H. Brown, On the possible presence of ice on the Moon. J. Geophys. Res. **66**(5), 1598–1600 (1961). https://doi.org/10.1029/JZ066i005p01598

K. Watson, B.C. Murray, H. Brown, The behavior of volatiles on the lunar surface. J. Geophys. Res. **66**(9), 3033–3045 (1961). https://doi.org/10.1029/JZ066i009p03033

J.-P. Williams, D.A. Paige, B.T. Greenhagen, E. Sefton-Nash, The global surface temperatures of the Moon as measured by the diviner Lunar radiometer experiment. Icarus **283**, 300–325 (2017). https://doi.org/10.1016/j.icarus.2016.08.012